

# On the Entire Structure of the Energy Bands of 1D Moiré Superchain

Dmitrii Vorobev, Stom (Yiheng) Chen and Grigory M. Tarnopolsky  
*Department of Physics, Carnegie Mellon University, Pittsburgh, PA 15213, USA*

We consider a general model of two atomic chains forming a moiré pattern due to a small mismatch in their lattice spacings, given by  $\theta = (a_1 - a_2)/a_2$ . Assuming arbitrary single-band dispersion relations  $\varepsilon_1(p)$  and  $\varepsilon_2(q)$  for the chains, along with an arbitrary inter-chain coupling term  $T(x)$ , we show that the entire spectrum of such a one-dimensional moiré superchain is governed by a single three-term recurrence (TTR) relation. We analyze this TTR relation using the discrete WKB method and demonstrate how the entire structure of the spectrum as well as emergence of flat bands can be easily identified from a pair of upper and lower potential functions of the TTR relation. We also comment on the chiral limit of the moiré superchain, which can be viewed, in some sense, as a 1D analog of the chiral limit of Twisted Bilayer Graphene.

## I. INTRODUCTION

The 2D moiré superlattices, as part of general van der Waals heterostructures, have recently become one of the mainstream research areas in modern condensed matter physics, both in experiments and theory [1–27]. Flat bands and magic angles in Twisted Bilayer Graphene (TBG) are among the most fascinating examples of intriguing new physics emerging in these complex structures. Recently, there has been progress in understanding the formation and properties of flat bands in TBG [28–34] and Twisted Graphene Multilayers [35–49]. Nevertheless, a general principle for analyzing and predicting the formation of flat bands in moiré lattices is not yet well understood.

In this article, we take a step toward a better understanding structure of the moiré bands by studying a simple yet general model of two one-dimensional chains of atoms with a small mismatch  $\theta = (a_1 - a_2)/a_2$  between their lattice spacings  $a_1$  and  $a_2$ , which together form a moiré superchain. This type of 1D superchain has been studied in many previous works [50–58] and a special case of the model we investigate was carefully analyzed in [51], from the perspective of the local density of states. In this article, we show that the entire structure of the moiré bands of such a superchain is governed by a single three-term recursion (TTR) relation. The small mismatch parameter  $\theta \ll 1$  enables the application of the discrete WKB method [59]. This method reveals that the band structure can be effectively analyzed using a pair of upper and lower potential functions of the TTR relation. We also note that a closely related 2D problem involves a 1D moiré pattern formed in the 2D superlattices due to lattice strain [28, 60, 61].

The article is organized as follows. In Section 2, we describe our model and derive its continuum Hamiltonian. In Section 3, we show how the moiré bands can be obtained by solving a single TTR relation. In Section 4, we demonstrate how the discrete WKB method reveals the entire structure of the moiré bands. Finally, in Section 5, we derive the semiclassical energy quantization conditions and explain the emergence of flat bands in certain energy regions of the spectrum.

## II. CONTINUUM MODEL FOR MOIRÉ SUPERCHAIN

Let us consider an electron that can hop along two 1D chains of atoms as well as between them, as shown in the Figure 1. We assume that individual chains have Hamil-

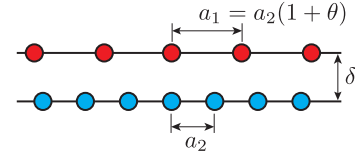


FIG. 1. Two one-dimensional chains of atoms with slightly different lattice spacings  $a_1$  and  $a_2$  form a moiré superchain. An electron can hop along each chain and between of them.

tonians  $H_1$  and  $H_2$  with single-band dispersion relations  $\varepsilon_1(p)$  and  $\varepsilon_2(q)$ , respectively. The inter-chain coupling term is given by  $T(x_n - y_m)$ , where  $x_n = na_1$  denotes the coordinate of atom  $n$  in the first chain, and  $y_m = ma_2$  denotes the coordinate of atom  $m$  in the second chain. The Hamiltonian for such an electron is given by

$$H = H_1 + H_2 + \sum_{n,m} (T(x_n - y_m) c_n^\dagger d_m + \text{H.c.}), \quad (1)$$

where  $c_n^\dagger, c_n$  and  $d_m^\dagger, d_m$  are the electron creation and annihilation operators,  $a_2 = a_1/(1 + \theta)$  and  $\theta$  is a small value, which encodes a lattice mismatch between the chains and is the 1D equivalent to the twist angle. As an example we can consider the inter-chain hopping term  $T(x)$  in one of the following forms:

$$T(x) = we^{-|x|/\xi}, \quad T(x) = we^{(\delta - \sqrt{x^2 + \delta^2})/\xi}, \quad (2)$$

or  $T(x) = we^{-x^2/\xi^2}$  as in [51, 53], where  $\xi$  is the correlation length parameter and  $\delta$  is a distance between the chains. We introduce creation and annihilation operators  $c_p^\dagger, c_p$  and  $d_q^\dagger, d_q$  in the momentum space using the formulas

$$c_p = \frac{1}{\sqrt{b_1}} \sum_n c_n e^{-ipx_n}, \quad d_q = \frac{1}{\sqrt{b_2}} \sum_m d_m e^{-iqy_m}, \quad (3)$$

where  $b_1 = 2\pi/a_1$  and  $b_2 = 2\pi/a_2$  are the inverse-lattice primitive vectors. Using the momentum space operators we find for the Hamiltonian

$$H = \int_0^{b_1} dp \varepsilon_1(p) c_p^\dagger c_p + \int_0^{b_2} dq \varepsilon_2(q) d_q^\dagger d_q + \int_0^{b_1} dp \int_0^{b_2} dq (T_{p,q} c_p^\dagger d_q + \text{H.c.}), \quad (4)$$

and we denoted by  $T_{p,q}$  the expression

$$T_{k,q} = \frac{1}{\sqrt{b_1 b_2}} \sum_{n,m} T(x_n - y_m) e^{-ikx_n + iqy_m}. \quad (5)$$

Let us define the continuous Fourier transform for the inter-chain hopping function  $T(x)$  as

$$T(p) \equiv \frac{1}{\sqrt{a_1 a_2}} \int_{-\infty}^{+\infty} dx T(x) e^{-ipx}, \quad (6)$$

and using this definition we obtain an expression for  $T_{k,q}$

$$T_{k,q} = \sum_{G_1, G_2} T(k - G_1) \delta(q - k + G_1 + G_2), \quad (7)$$

where  $G_1 = m_1 b_1$  and  $G_2 = m_2 b_2$  are inverse lattice vectors of the first and second chains. Therefore the Hamiltonian reads

$$H = \int_0^{b_1} dp \varepsilon_1(p) c_p^\dagger c_p + \int_0^{b_2} dq \varepsilon_2(q) d_q^\dagger d_q + \int_0^{b_1} dp \left( \sum'_{G_1, G_2} T(p - G_1) c_p^\dagger d_{p - G_1 - G_2} + \text{H.c.} \right), \quad (8)$$

where  $\sum'_{G_1, G_2}$  indicates that we sum only over those  $G_1$  and  $G_2$  for which  $p - G_1 - G_2$  lies within the interval  $\text{BZ}_2 = [0, b_2]$ , the Brillouin zone for the  $q$  momentum.

Without loss of generality we assume that  $a_2 < a_1$ , and thus  $b_2 > b_1$ . We also assume that the function  $T(p)$  decays rapidly with  $p$  and has its maximum at  $p = 0$ . Therefore,  $T(p - G_1)$  takes its largest values only for  $G_1 = 0$  and  $G_1 = -b_1$ , so these are the terms we retain in the continuum model Hamiltonian

$$H_{\text{cont}} = \int_0^{b_1} dp \varepsilon_1(p) c_p^\dagger c_p + \int_0^{b_2} dq \varepsilon_2(q) d_q^\dagger d_q + \sum'_{G_2} \int_0^{b_1} dp (T(p) c_p^\dagger d_{p - G_2} + T(p - b_1) c_p^\dagger d_{p - b_1 - G_2} + \text{H.c.}). \quad (9)$$

Finally, since  $p - G_2$  in the first inter-chain term must belong to the interval  $\text{BZ}_2 = [0, b_2]$ , and since  $p \in \text{BZ}_1 = [0, b_1]$ , we must take only  $G_2 = 0$ . Similarly,  $p - b_1 - G_2$  in the second term lies in the interval  $\text{BZ}_2 = [0, b_2]$  only if  $G_2 = -b_2$ . Thus, we finally find

$$H_{\text{cont}} = \int_0^{b_1} dp \varepsilon_1(p) c_p^\dagger c_p + \int_0^{b_2} dq \varepsilon_2(q) d_q^\dagger d_q + \int_0^{b_1} dp (T(p) c_p^\dagger d_p + T(p - b_1) c_p^\dagger d_{p + b_m} + \text{H.c.}), \quad (10)$$

where we denoted by  $b_m \equiv b_2 - b_1$  the moiré inverse unit vector, depicted in Figure 2. We notice that  $b_2 = b_1(1 + \theta)$

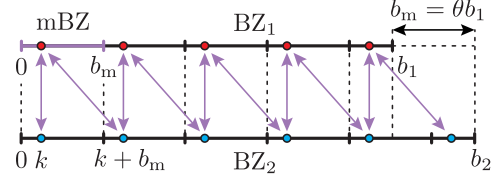


FIG. 2. Two Brillouin zones  $\text{BZ}_1$  and  $\text{BZ}_2$  of the first and second chains and the moiré vector  $b_m \equiv b_2 - b_1$ . The moiré Bloch vector  $k$  belongs to the moiré Brillouin zone  $\text{mBZ} = [0, b_m]$  and the momenta  $k + jb_m$ ,  $j = 0, 1, \dots, n_m$  of the  $\text{BZ}_1$  and  $\text{BZ}_2$  are coupled by the continuum Hamiltonian (10).

and therefore  $b_m = \theta b_1$  with  $\theta \ll 1$ . The continuum model (10) is accurate, provided that the inter-chain hopping term  $T(p)$  decays rapidly on the scale of  $b_1$ , so that the terms neglected in the sum over  $G_1$  in (8) are small.

We see that the momenta  $k + jb_m$ , with  $j = 0, 1, 2, \dots$  of the  $\text{BZ}_1$  and  $\text{BZ}_2$  are coupled to each other by the continuum model Hamiltonian (10) as shown in the Figure 2. In general we assume that  $b_1 = n_m b_m + r b_m$ , where  $n_m$  is a number of full moiré Brillouin zones  $\text{mBZ} = [0, b_m]$  inside  $\text{BZ}_1$  and  $0 \leq r < 1$  is the reminder. If  $r > 0$ , then for the first interval  $k \in [0, r b_m]$  of  $\text{mBZ}$  we have  $j = 0, 1, 2, \dots, n_m$  and for the second interval  $k \in [r b_m, b_m]$  we have  $j = 0, 1, 2, \dots, n_m - 1$  for  $\text{BZ}_1$  and  $\text{BZ}_2$  has always one extra mode. For simplicity below we assume a commensurate case, when there are exactly integer number  $n_m$  of the moiré vectors  $b_m$  inside  $b_1$ , so the reminder  $r = 0$ . In this case the moiré Hamiltonian is a block matrix of the form

$$H_{\text{moiré}}(k) = \begin{pmatrix} H_1(k) & T(k) \\ T^\dagger(k) & H_2(k) \end{pmatrix}, \quad (11)$$

where  $k \in \text{mBZ} = [0, b_m]$  and  $H_1(k)_{j,j'} = \varepsilon_1(k + j b_m) \delta_{j,j'}$  with  $j = 0, \dots, n_m - 1$  and  $H_2(k)_{j,j'} = \varepsilon_2(k + j b_m) \delta_{j,j'}$  with  $j = 0, \dots, n_m$  are diagonal matrices representing intra-chain dispersion relations and  $T(k)$  is  $n_m \times (n_m + 1)$  inter-chain hopping matrix that has only diagonal and upper diagonal non-zero elements:  $T(k)_{j,j} = T(k + j b_m)$  and  $T(k)_{j,j+1} = T(k + j b_m - b_1)$ .

We notice that if we consider the limit when the intra-chain terms are zero,  $H_1 = H_2 = 0$ , then the Hamiltonian (11) has chiral symmetry and hosts an exact flat band at zero energy. This flat band arises from the fact that the matrix  $T$  has one more column than rows, and thus has exactly one zero mode for each  $k$ . This 1D limit can be viewed, in some sense, as a 1D analog of the chiral limit of TBG [28, 29]. We demonstrate below that this flat band is stable under small nonzero intra-chain terms  $H_1$  and  $H_2$ , while the discrete WKB method does not capture it.

### III. MOIRÉ BANDS AND THREE-TERM RECURRENCE RELATION

To find the moiré bands we solve the static Schrödinger equation

$$H_{\text{moiré}}(k)|\psi_n(k)\rangle = \varepsilon_{nk}|\psi_n(k)\rangle, \quad (12)$$

for every  $k \in \text{mBZ} = [0, b_m]$ , where  $n$  is the band index. The equation (12) can be written explicitly in components  $\mathbf{u} = (u_0, \dots, u_{n_m-1})$  and  $\mathbf{v} = (v_0, \dots, v_{n_m})$  of the vector  $|\psi(k)\rangle = (\mathbf{u}, \mathbf{v})^T$ , as

$$\begin{cases} \varepsilon_{1,j}u_j + t_jv_j + \tilde{t}_jv_{j+1} = \varepsilon u_j \\ \varepsilon_{2,j}v_j + t_ju_j + \tilde{t}_{j-1}u_{j-1} = \varepsilon v_j \end{cases}, \quad (13)$$

where we suppressed indices  $n$  and  $k$  for brevity and also introduced short notations  $\varepsilon_{1,2;j} \equiv \varepsilon_{1,2}(k + jb_m)$  and

$$t_j \equiv T(k + jb_m), \quad \tilde{t}_j \equiv T(k + jb_m - b_1). \quad (14)$$

Using the first equation in (13) to express  $u_j$  in terms of  $v_j$  and  $v_{j+1}$ , and substituting it into the second equation, we obtain a single equation for  $v_j$  in the form

$$\mu_j v_{j-1} + w_j v_j + \mu_{j+1} v_{j+1} = 0, \quad (15)$$

where  $j = 0, \dots, n_m$ ; we assume  $v_{-1} = v_{n_m+1} = 0$  and we introduced  $\mu_j \equiv t_{j-1}\tilde{t}_{j-1}/(\varepsilon - \varepsilon_{1,j-1})$  and

$$w_j \equiv \frac{t_j^2}{\varepsilon - \varepsilon_{1,j}} + \frac{\tilde{t}_{j-1}^2}{\varepsilon - \varepsilon_{1,j-1}} - (\varepsilon - \varepsilon_{2,j}). \quad (16)$$

Equivalently one can obtain a similar equation for the components  $u_j$ . The equation (15) is called a three-term recurrence (TTR) relation and is ubiquitous in physics and mathematics. This TTR can also be represented as a eigenvalue equation with a zero eigenvalue for a finite Hermitian Jacobi (tridiagonal) matrix [62].

For the moiré superchain we assume that the lattice mismatch parameter  $\theta = b_m/b_1 \ll 1$  is small. In this case, the coefficients  $\mu_j$  and  $w_j$  vary slowly with  $j$ , which allows us to apply the discrete WKB method [59, 63–67] to the TTR relation (15) and to determine the entire moiré spectrum  $\varepsilon$  both qualitatively and quantitatively.

### IV. ENTIRE STRUCTURE OF THE MOIRÉ BANDS

In this section, we rely mostly on the results and some notations presented in [59, 66]. We first discuss qualitatively the structure of the energy levels determined by the TTR relation (15). At the leading level of accuracy we ignore  $O(\theta)$  order corrections, and therefore can make approximations  $\varepsilon_{1,j-1} \approx \varepsilon_{1,j}$  and  $\tilde{t}_{j-1} \approx \tilde{t}_j$  in the coefficients  $\mu_j$  and  $w_j$  and we also take the Bloch vector  $k = 0$ . This allows to rewrite (15) in a simpler form

$$\tilde{\mu}_j v_{j-1} + \tilde{w}_j v_j + \tilde{\mu}_{j+1} v_{j+1} = 0, \quad (17)$$

where  $\tilde{\mu}_j \equiv t_j \tilde{t}_j$  and  $\tilde{w}_j = t_j^2 + \tilde{t}_j^2 - (\varepsilon - \varepsilon_{1,j})(\varepsilon - \varepsilon_{2,j})$ . Solving the equations  $\tilde{w}_j \pm 2\tilde{\mu}_j = 0$  with respect to energy  $\varepsilon$  we obtain two lower  $U_{1,j}^-$ ,  $U_{2,j}^-$  and two upper  $U_{1,j}^+$ ,  $U_{2,j}^+$  potential functions for the energy  $\varepsilon$ :

$$U_{1,j}^\pm = \frac{\varepsilon_{1,j} + \varepsilon_{2,j}}{2} - \sqrt{\frac{(\varepsilon_{1,j} - \varepsilon_{2,j})^2}{4} + (t_j \mp \tilde{t}_j)^2}, \quad (18)$$

$$U_{2,j}^\pm = \frac{\varepsilon_{1,j} + \varepsilon_{2,j}}{2} + \sqrt{\frac{(\varepsilon_{1,j} - \varepsilon_{2,j})^2}{4} + (t_j \pm \tilde{t}_j)^2}, \quad (19)$$

and we notice that for any  $j$  the potential functions obey the chain of inequalities

$$U_{1,j}^- < U_{1,j}^+ \leq \varepsilon_{1,j}, \varepsilon_{2,j} \leq U_{2,j}^- < U_{2,j}^+. \quad (20)$$

For a given energy  $\varepsilon$ , the classically allowed values of  $j$  are determined by the inequalities

$$U_{1,j}^- < \varepsilon < U_{1,j}^+, \quad U_{2,j}^- < \varepsilon < U_{2,j}^+, \quad (21)$$

where, from now on, we treat the discrete variable  $j$  as a continuous one. Here, we can already notice the difference from the usual WKB approach, in which a single potential function  $U(x)$  defines the classically allowed and forbidden regions of a particle's motion. In the discrete WKB method, the momentum operator  $\hat{p} = -i\partial/\partial j$  enters the TTR relation as  $\mu_{j+1/2} \cos \hat{p}$  at the  $O(\theta)$  order of accuracy, which leads to the upper and lower potential functions [59]. We note that, in the usual TTR relation, the energy  $\varepsilon$  enters the equation linearly [59]. However, in our case,  $\varepsilon$  enters the relation nonlinearly through the coefficients  $\mu_j$  and  $w_j$ , giving rise to a pair of lower and upper potential functions. Nevertheless, the discrete WKB method remains conceptually unchanged.

The intervals of possible values of quantized energies  $\varepsilon$  are bound by minimums of  $U_{1,j}^-$  and  $U_{2,j}^-$  and maximums of  $U_{1,j}^+$  and  $U_{2,j}^+$ :

$$\begin{aligned} \min_j U_{1,j}^- &\leq \varepsilon \leq \max_j U_{1,j}^+, \\ \min_j U_{2,j}^- &\leq \varepsilon \leq \max_j U_{2,j}^+. \end{aligned} \quad (22)$$

In fact one can rigorously prove [67] that quantized energies  $\varepsilon$  must satisfy the inequalities

$$\begin{aligned} \min_j (w_j - |\mu_j| - |\mu_{j+1}|) &\leq 0 \\ \max_j (w_j + |\mu_j| + |\mu_{j+1}|) &\geq 0, \end{aligned} \quad (23)$$

and this coincides with (22) at the order  $O(\theta)$ .

As an example in Figure 3 we plot  $U_{1,j}^-$ ,  $U_{1,j}^+$  and  $U_{2,j}^-$ ,  $U_{2,j}^+$  functions together with the moiré bands obtained from exact numerical solution of (15), for a particular case when  $\varepsilon_1(p) = \cos(pa_1)$ ,  $\varepsilon_2(q) = 0.5 \cos(qa_2)$  and

$$T(p) = 2w\sqrt{1 + \theta} \frac{\xi/a_1}{1 + p^2\xi^2}, \quad (24)$$

which is the Fourier transform (6) of the interchain hopping function  $T(x) = we^{-|x|/\xi}$  with  $w = 3/2$  and

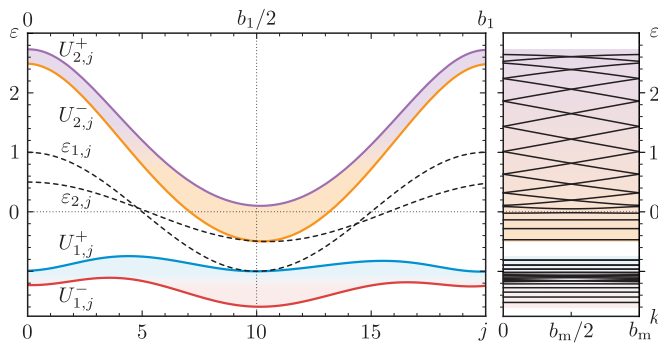


FIG. 3. (Left) Plot of the potential functions  $U_{1,j}^-, U_{1,j}^+$  and  $U_{2,j}^-, U_{2,j}^+$  (solid colored lines) and dispersions  $\varepsilon_{1,j}$  and  $\varepsilon_{2,j}$  (black dashed lines) for the case  $\varepsilon_1(p) = \cos(pa_1)$ ,  $\varepsilon_2(q) = 0.5 \cos(qa_2)$  and  $T(p)$  in (24) with  $w = 3/2$ ,  $\xi/a_1 = 0.6$  and  $\theta = 0.05$ , with highlighted classically allowed regions of energy. (Right) Moiré bands obtained from exact numerical solution of (15).

$\xi/a_1 = 0.6$  and  $\theta = 0.05$ . We notice that the mismatch parameter  $\theta$  enters inter-chain hopping function  $T(p)$  via the factor  $1/\sqrt{a_1 a_2}$  in (6). One can clearly see from this plot that the exact moiré spectrum obeys inequalities (22). We can also observe several regions of highly flat bands as well as the regions where bands strongly depend on the moiré Bloch vector  $k$ . We explain it in the next section by analysing solution of the TTR relation (15) using Bohr–Sommerfeld quantization conditions for the discrete WKB method.

## V. MOIRÉ BANDS FROM THE DISCRETE WKB METHOD

To apply the discrete WKB method to the TTR relation (15) we treat the discrete variable  $j$  as continuous one. Following [59, 66] we define two types of the turning points: a “usual” turning point  $j_t$  is defined as the point where  $\varepsilon = U_{j_t}^+$  and an “unusual” turning point corresponds to  $\varepsilon = U_{j_t}^-$ . In our case since the energy  $\varepsilon$  enters TTR implicitly through  $\mu_j$  and  $w_j$  we find the left and right turning points  $j_l$  and  $j_r$  by solving the equations:

$$w_j \pm 2\sqrt{\mu_j \mu_{j+1}} = 0 \quad (25)$$

with respect to  $j$  for a fixed energy  $\varepsilon$ .<sup>1</sup> Now we are working at the accuracy  $O(\theta)$ , therefore we can not make approximations similar to those when we obtained (17). The Bohr–Sommerfeld quantization rules for the discrete WKB method depend on the type of the turning points, and thus there are four different cases. The quantization

rules for these cases are [59]:

$$\int_{j_l}^{j_r} dj \phi_j = \pi n + \begin{cases} \frac{\pi}{2} + \pi(j_r - j_l), & j_l, j_r \in U^- \\ -\pi j_l, & j_l \in U^-, j_r \in U^+ \\ \pi j_r, & j_l \in U^+, j_r \in U^- \\ \frac{\pi}{2}, & j_l, j_r \in U^+ \end{cases}, \quad (26)$$

where  $n$  is a positive or negative integer and the functions  $\phi_j$  and  $\Pi_j$  are defined as

$$\phi_j \equiv \arccos(\Pi_j), \quad \Pi_j \equiv -\frac{w_j}{2\sqrt{\mu_j \mu_{j+1}}}. \quad (27)$$

The quantization equations (26) are the transcendental equations which define quantized values of energy  $\varepsilon$ , which in turn enters inside the function  $\Pi_j$  and the turning points  $j_l, j_r$ . The equations (26) are written to  $O(\theta^0)$  accuracy, omitting  $O(\theta)$  terms. This implies that the function  $\phi_j$  is accurate up to  $O(\theta)$ , since the turning points  $j_l$  and  $j_r$  are of order  $O(\theta^{-1})$ . In general, we expect the energy spacings to be of order  $O(\theta)$ .

In our case since  $j$  runs over the finite interval  $[0, n_m]$ , there are also possible cases when an energy level  $\varepsilon$  lacks a left turning point, or a right turning point, or both. Therefore we have five additional quantization rules:

$$\int_{j_l}^{j_r} dj \phi_j = \pi n - \begin{cases} \phi_0 + \frac{\pi}{4}, & j_l = 0, j_r \in U^+ \\ \phi_0 - \pi j_r - \frac{\pi}{4}, & j_l = 0, j_r \in U^- \\ \phi_{n_m} + \frac{\pi}{4}, & j_l \in U^+, j_r = n_m \\ \phi_{n_m} + \pi j_l - \frac{\pi}{4}, & j_l \in U^-, j_r = n_m \\ \phi_0 + \phi_{n_m}, & j_l = 0, j_r = n_m \end{cases}$$

We note that, due to the inequalities in (20), the energy  $\varepsilon$  does not cross the dispersion  $\varepsilon_{1,j}$  in the classically allowed regions, therefore we need not worry about potential singularities in the coefficients  $\mu_j$  and  $w_j$ .

Finally, we explain the appearance of flat bands in certain regions of the moiré bands. First, we note that the moiré Bloch vector  $k$  enters the coefficients  $w_j$  and  $\mu_j$  in the combination  $k + j b_m$ . Now, consider the case in which the left and right turning points  $j_l, j_r$  both belong to  $U^-$  or both belong to  $U^+$ . In these two cases, the vector  $k$  can be excluded from the quantization equations (26) by the shift  $j \rightarrow j - k/b_m$ . Therefore the quantized energies  $\varepsilon$  are independent on  $k$  up to order  $O(\theta^2)$ . Actually, one can show that, due to the localization of the wave functions in real space, some of these flat bands have an exponentially small bandwidth [68], similar to the lower-energy bands of the Mathieu equation [69, 70]. In the Figure 3 we can clearly see that flat bands indeed appear in the energy range, where the turning points  $j_l, j_r$  both belong to either  $U^-$  or to  $U^+$  potential functions.

In contrast, if the turning points  $j_l$  and  $j_r$  belong to different types of the potential functions, then the quantization equations (26) depend on the “unusual” turning point. In that case, the shift  $j \rightarrow j - k/b_m$  removes the vector  $k$  from the left-hand side of (26), but  $k$  reappears explicitly as  $\pi(n \pm k/b_m)$  on the right-hand side of (26),

<sup>1</sup> We emphasize again that we treat  $j$  as a continuous variable and that  $j_l$  and  $j_r$  are real numbers (not necessarily integers).

causing the quantized energy to strongly depend on  $k$  and form a zigzag-like energy bands pattern. This behavior is also clearly observed in Figure 3.

In order to demonstrate how the quantization rules (26) work in practice, we plot Figure 4 with parameters:  $\varepsilon_1(p) = 2 \cos(pa_1)$ ,  $\varepsilon_2(q) = \cos(qa_2)$ , and  $T(p)$  as in (24) with  $w = 10$ ,  $\xi/a_1 = 0.6$ , and  $\theta = 0.05$ . On the right side of the figure, we plot the exact moiré bands (solid black lines) together with the bands obtained from the quantization rules (26) (dashed colored lines). We see that the accuracy is indeed of order  $O(\theta^2)$ , and the difference between the exact bands and the WKB ones is almost invisible. We also notice that the energy level near zero is a remnant of the chiral limit flat band discussed at the end of Section II and is not captured by the quantization rules (26).

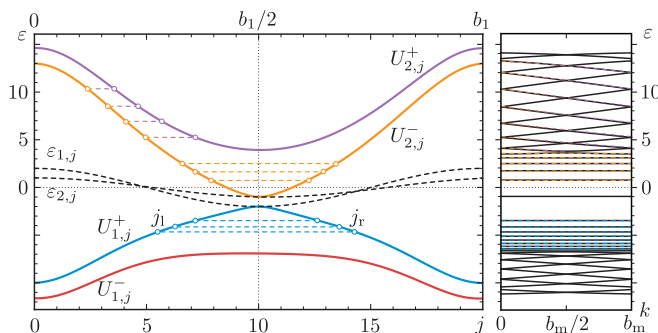


FIG. 4. (Left) Plot of the potential functions  $U_{1,j}^-$ ,  $U_{1,j}^+$  and  $U_{2,j}^-$ ,  $U_{2,j}^+$  (solid colored lines) along with the dispersions  $\varepsilon_{1,j}$  and  $\varepsilon_{2,j}$  (black dashed lines) for the case  $\varepsilon_1(p) = 2 \cos(pa_1)$ ,  $\varepsilon_2(q) = \cos(qa_2)$ , and  $T(p)$  in (24), with  $w = 10$ ,  $\xi/a_1 = 0.6$ , and  $\theta = 0.05$ . We also plot a few classical energy levels (dashed colored lines) along with their turning points,  $j_l$  and  $j_r$ . (Right) Exact moiré bands (solid black lines) together with bands obtained from the quantization rules (26) (dashed colored lines). The energy level near zero is a remnant of the chiral limit flat band and is not captured by (26).

## VI. CONCLUSIONS

In this article, we showed how the discrete WKB method can reveal the entire structure of the moiré super-chain energy spectrum and explain the emergence of flat bands. By simply constructing the upper and lower potential curves at leading order of accuracy one can qualitatively understand the complete moiré spectrum and identify regions where narrow bands arise. One can also use the potential functions to inverse-engineer the desired moiré bands by tuning the intra- and inter-chain hopping parameters. We leave a more detailed analysis of the band structure and the stability of the chiral limit flat band, for specific dispersion relations and inter-chain hopping terms in this model, to future work [68]. We also notice that instead of two chains, one can consider three or more nearby chains of atoms, similar to the 2D multilayers.

It would be interesting to further investigate the role of interactions in the one-dimensional moiré superchain, depending on the filling factor [71]. Finally, we point out that the discrete WKB method is mostly developed for only one-dimensional TTR relations. It would be valuable to generalize these ideas to two-dimensional moiré superlattices, which could potentially clarify the fundamental principles governing the formation and stability of flat bands in the 2D case.

## ACKNOWLEDGMENTS

We are grateful to Shubhayu Chatterjee, Mitchell Luskin, Tina Kahniashvili, Igor R. Klebanov and Vlad Kozii for very useful discussions. We would also like to thank Igor R. Klebanov for his valuable comments on the draft.

- 
- [1] Y. Cao, V. Fatemi, S. Fang, K. Watanabe, T. Taniguchi, E. Kaxiras, and P. Jarillo-Herrero, “Unconventional superconductivity in magic-angle graphene superlattices,” *Nature*, vol. 556, no. 7699, pp. 43–50, 2018.
  - [2] Y. Cao, V. Fatemi, A. Demir, S. Fang, S. L. Tomarken, J. Y. Luo, J. D. Sanchez-Yamagishi, K. Watanabe, T. Taniguchi, E. Kaxiras, R. C. Ashoori, and P. Jarillo-Herrero, “Correlated insulator behaviour at half-filling in magic-angle graphene superlattices,” *Nature*, vol. 556, no. 7699, pp. 80–84, 2018.
  - [3] M. Yankowitz, S. Chen, H. Polshyn, K. Watanabe, T. Taniguchi, D. Graf, A. F. Young, and C. R. Dean, “Tuning superconductivity in twisted bilayer graphene,” *arXiv:1808.07865*, 2018.
  - [4] G. Li, A. Luican, J. M. B. Lopes dos Santos, A. H. Castro Neto, A. Reina, J. Kong, and E. Y. Andrei, “Observation of van hove singularities in twisted graphene layers,” *Nature Physics*, vol. 6, pp. 109–113, February 2010.
  - [5] R. Bistritzer and A. H. MacDonald, “Moiré bands in twisted double-layer graphene,” *Proceedings of the National Academy of Sciences*, vol. 108, no. 30, pp. 12233–



- 12237, 2011.
- [6] E. Suárez Morell, J. D. Correa, P. Vargas, M. Pacheco, and Z. Barticevic, “Flat bands in slightly twisted bilayer graphene: Tight-binding calculations,” *Phys. Rev. B*, vol. 82, p. 121407, Sep 2010.
- [7] H. C. Po, L. Zou, A. Vishwanath, and T. Senthil, “Origin of mott insulating behavior and superconductivity in twisted bilayer graphene,” *Phys. Rev. X*, vol. 8, p. 031089, Sep 2018.
- [8] A. Thomson, S. Chatterjee, S. Sachdev, and M. S. Scheurer, “Triangular antiferromagnetism on the honeycomb lattice of twisted bilayer graphene,” *Phys. Rev. B*, vol. 98, p. 075109, Aug 2018.
- [9] L. Zou, H. C. Po, A. Vishwanath, and T. Senthil, “Band structure of twisted bilayer graphene: Emergent symmetries, commensurate approximants, and wannier obstructions,” *Phys. Rev. B*, vol. 98, p. 085435, Aug 2018.
- [10] D. K. Efimkin and A. H. MacDonald, “Helical network model for twisted bilayer graphene,” *Phys. Rev. B*, vol. 98, p. 035404, Jul 2018.
- [11] N. F. Q. Yuan and L. Fu, “Model for the metal-insulator transition in graphene superlattices and beyond,” *Phys. Rev. B*, vol. 98, p. 045103, Jul 2018.
- [12] C. Xu and L. Balents, “Topological superconductivity in twisted multilayer graphene,” *Phys. Rev. Lett.*, vol. 121, p. 087001, Aug 2018.
- [13] M. Ochi, M. Koshino, and K. Kuroki, “Possible correlated insulating states in magic-angle twisted bilayer graphene under strongly competing interactions,” *Phys. Rev. B*, vol. 98, p. 081102, Aug 2018.
- [14] F. Wu, A. H. MacDonald, and I. Martin, “Theory of phonon-mediated superconductivity in twisted bilayer graphene,” *Phys. Rev. Lett.*, vol. 121, p. 257001, Dec 2018.
- [15] Y.-H. Zhang, D. Mao, Y. Cao, P. Jarillo-Herrero, and T. Senthil, “Nearly flat chern bands in moiré superlattices,” *Phys. Rev. B*, vol. 99, p. 075127, Feb 2019.
- [16] J. Kang and O. Vafek, “Symmetry, maximally localized wannier states, and a low-energy model for twisted bilayer graphene narrow bands,” *Phys. Rev. X*, vol. 8, p. 031088, Sep 2018.
- [17] J. M. Pizarro, M. J. Calderón, and E. Bascones, “The nature of correlations in the insulating states of twisted bilayer graphene,” *Journal of Physics Communications*, vol. 3, p. 035024, mar 2019.
- [18] M. Koshino, N. F. Q. Yuan, T. Koretsune, M. Ochi, K. Kuroki, and L. Fu, “Maximally localized wannier orbitals and the extended hubbard model for twisted bilayer graphene,” *Phys. Rev. X*, vol. 8, p. 031087, Sep 2018.
- [19] D. M. Kennes, J. Lischner, and C. Karrasch, “Strong correlations and  $d + id$  superconductivity in twisted bilayer graphene,” *Phys. Rev. B*, vol. 98, p. 241407, Dec 2018.
- [20] H. Isobe, N. F. Q. Yuan, and L. Fu, “Unconventional superconductivity and density waves in twisted bilayer graphene,” *Phys. Rev. X*, vol. 8, p. 041041, Dec 2018.
- [21] L. Rademaker and P. Mellado, “Charge-transfer insulation in twisted bilayer graphene,” *Phys. Rev. B*, vol. 98, p. 235158, Dec 2018.
- [22] T. J. Peltonen, R. Ojajärvi, and T. T. Heikkilä, “Mean-field theory for superconductivity in twisted bilayer graphene,” *Phys. Rev. B*, vol. 98, p. 220504, Dec 2018.
- [23] V. Kozii, H. Isobe, J. W. F. Venderbos, and L. Fu, “Nematic superconductivity stabilized by density wave fluctuations: Possible application to twisted bilayer graphene,” *Phys. Rev. B*, vol. 99, p. 144507, Apr 2019.
- [24] V. Kozii, M. P. Zaletel, and N. Bultinck, “Spin-triplet superconductivity from intervalley goldstone modes in magic-angle graphene,” *Phys. Rev. B*, vol. 106, p. 235157, Dec 2022.
- [25] Z. Song, Z. Wang, W. Shi, G. Li, C. Fang, and B. A. Bernevig, “All magic angles in twisted bilayer graphene are topological,” *Phys. Rev. Lett.*, vol. 123, p. 036401, Jul 2019.
- [26] K. Hejazi, C. Liu, H. Shapourian, X. Chen, and L. Balents, “Multiple topological transitions in twisted bilayer graphene near the first magic angle,” *Phys. Rev. B*, vol. 99, p. 035111, Jan 2019.
- [27] H. C. Po, L. Zou, T. Senthil, and A. Vishwanath, “Faithful tight-binding models and fragile topology of magic-angle bilayer graphene,” *Phys. Rev. B*, vol. 99, p. 195455, May 2019.
- [28] P. San-Jose, J. González, and F. Guinea, “Non-abelian gauge potentials in graphene bilayers,” *Phys. Rev. Lett.*, vol. 108, p. 216802, May 2012.
- [29] G. Tarnopolsky, A. J. Kruchkov, and A. Vishwanath, “Origin of magic angles in twisted bilayer graphene,” *Phys. Rev. Lett.*, vol. 122, p. 106405, Mar 2019.
- [30] P. J. Ledwith, G. Tarnopolsky, E. Khalaf, and A. Vishwanath, “Fractional chern insulator states in twisted bilayer graphene: An analytical approach,” *Phys. Rev. Res.*, vol. 2, p. 023237, May 2020.
- [31] F. K. Popov and A. Milekhin, “Hidden wave function of twisted bilayer graphene: The flat band as a landau level,” *Phys. Rev. B*, vol. 103, p. 155150, Apr 2021.
- [32] J. Wang, Y. Zheng, A. J. Millis, and J. Cano, “Chiral approximation to twisted bilayer graphene: Exact intravalley inversion symmetry, nodal structure, and implications for higher magic angles,” *Phys. Rev. Res.*, vol. 3, p. 023155, May 2021.
- [33] J. Wang, J. Cano, A. J. Millis, Z. Liu, and B. Yang, “Exact landau level description of geometry and interaction in a flatband,” *Phys. Rev. Lett.*, vol. 127, p. 246403, Dec 2021.
- [34] Y. Sheffer, R. Queiroz, and A. Stern, “Symmetries as the guiding principle for flattening bands of dirac fermions,” *Phys. Rev. X*, vol. 13, p. 021012, Apr 2023.
- [35] E. Khalaf, A. J. Kruchkov, G. Tarnopolsky, and A. Vishwanath, “Magic angle hierarchy in twisted graphene multilayers,” *Phys. Rev. B*, vol. 100, p. 085109, Aug 2019.
- [36] C. Mora, N. Regnault, and B. A. Bernevig, “Flatbands and perfect metal in trilayer moiré graphene,” *Phys. Rev. Lett.*, vol. 123, p. 026402, Jul 2019.
- [37] T. Cea, N. R. Walet, and F. Guinea, “Twists and the electronic structure of graphitic materials,” *Nano Letters*, vol. 19, pp. 8683–8689, 12 2019.
- [38] Z. Zhu, S. Carr, D. Massatt, M. Luskin, and E. Kaxiras, “Twisted trilayer graphene: A precisely tunable platform for correlated electrons,” *Phys. Rev. Lett.*, vol. 125, p. 116404, Sep 2020.
- [39] X. Lin, C. Li, K. Su, and J. Ni, “Energetic stability and spatial inhomogeneity in the local electronic structure of relaxed twisted trilayer graphene,” *Physical Review B*, vol. 106, no. 7, p. 075423, 2022.
- [40] Z. Ma, S. Li, M. Lu, D.-H. Xu, J.-H. Gao, and X. Xie, “Doubled moiré flat bands in double-twisted few-layer graphite,” *Science China Physics, Mechanics & Astronomy*, vol. 66, no. 2, p. 227211, 2023.

- [41] M. Liang, M.-M. Xiao, Z. Ma, and J.-H. Gao, “Moiré band structures of the double twisted few-layer graphene,” *Phys. Rev. B*, vol. 105, p. 195422, May 2022.
- [42] P. J. Ledwith, A. Vishwanath, and E. Khalaf, “Family of ideal chern flatbands with arbitrary chern number in chiral twisted graphene multilayers,” *Phys. Rev. Lett.*, vol. 128, p. 176404, Apr 2022.
- [43] Y. Mao, D. Guerci, and C. Mora, “Supermoiré low-energy effective theory of twisted trilayer graphene,” *Phys. Rev. B*, vol. 107, p. 125423, Mar 2023.
- [44] F. K. Popov and G. Tarnopolsky, “Magic angles in equal-twist trilayer graphene,” *Phys. Rev. B*, vol. 108, p. L081124, Aug 2023.
- [45] D. Guerci, Y. Mao, and C. Mora, “Chern mosaic and ideal flat bands in equal-twist trilayer graphene,” *Phys. Rev. Res.*, vol. 6, p. L022025, Apr 2024.
- [46] T. Devakul, P. J. Ledwith, L.-Q. Xia, A. Uri, S. C. de la Barrera, P. Jarillo-Herrero, and L. Fu, “Magic-angle helical trilayer graphene,” *Science Advances*, vol. 9, no. 36, p. eadi6063, 2023.
- [47] N. Nakatsuji, T. Kawakami, and M. Koshino, “Multiscale lattice relaxation in general twisted trilayer graphenes,” *Phys. Rev. X*, vol. 13, p. 041007, Oct 2023.
- [48] F. K. Popov and G. Tarnopolsky, “Magic angle butterfly in twisted trilayer graphene,” *Phys. Rev. Res.*, vol. 5, p. 043079, Oct 2023.
- [49] D. Guerci, Y. Mao, and C. Mora, “Nature of even and odd magic angles in helical twisted trilayer graphene,” *Phys. Rev. B*, vol. 109, p. 205411, May 2024.
- [50] E. Cancès, P. Cazeaux, and M. Luskin, “Generalized kubo formulas for the transport properties of incommensurate 2d atomic heterostructures,” *Journal of Mathematical Physics*, vol. 58, June 2017.
- [51] S. Carr, D. Massatt, M. Luskin, and E. Kaxiras, “Duality between atomic configurations and bloch states in twistrionic materials,” *Phys. Rev. Res.*, vol. 2, p. 033162, Jul 2020.
- [52] G. A. Tritsarlis, S. Carr, and G. R. Schleder, “Computational design of moiré assemblies aided by artificial intelligence,” *Applied Physics Reviews*, vol. 8, p. 031401, 07 2021.
- [53] M. Gonçalves, B. Amorim, E. Castro, and P. Ribeiro, “Hidden dualities in 1d quasiperiodic lattice models,” *SciPost Physics*, vol. 13, Sept. 2022.
- [54] D. Liu, M. Luskin, and S. Carr, “Seeing moiré: Convolutional network learning applied to twistrionics,” *Phys. Rev. Res.*, vol. 4, p. 043224, Dec 2022.
- [55] D. X. Nguyen, X. Letartre, E. Drouard, P. Viktorovitch, H. C. Nguyen, and H. S. Nguyen, “Magic configurations in moiré superlattice of bilayer photonic crystals: Almost-perfect flatbands and unconventional localization,” *Phys. Rev. Res.*, vol. 4, p. L032031, Aug 2022.
- [56] D. Dams, D. Beutel, X. Garcia-Santiago, C. Rockstuhl, and R. Alaee, “Moiré flat bands in strongly coupled atomic arrays,” *Opt. Mater. Express*, vol. 13, pp. 2003–2019, Jul 2023.
- [57] G. R. Schleder, M. Pizzochero, and E. Kaxiras, “One-dimensional moiré physics and chemistry in heterostructured bilayer graphene,” *The Journal of Physical Chemistry Letters*, vol. 14, p. 8853–8858, Sept. 2023.
- [58] D. Vu and S. Das Sarma, “Generic mobility edges in several classes of duality-breaking one-dimensional quasiperiodic potentials,” *Phys. Rev. B*, vol. 107, p. 224206, Jun 2023.
- [59] P. A. Braun, “Discrete semiclassical methods in the theory of rydberg atoms in external fields,” *Rev. Mod. Phys.*, vol. 65, pp. 115–161, Jan 1993.
- [60] A. Timmel and E. J. Mele, “Dirac-harper theory for one-dimensional moiré superlattices,” *Phys. Rev. Lett.*, vol. 125, p. 166803, Oct 2020.
- [61] E. Andrade, F. López-Urías, and G. G. Naumis, “Topological origin of flat bands as pseudo-landau levels in uniaxial strained graphene nanoribbons and induced magnetic ordering due to electron-electron interactions,” *Phys. Rev. B*, vol. 107, p. 235143, Jun 2023.
- [62] F. R. Gantmacher and M. Krein, “Oscillation matrices and kernels and small vibrations of mechanical systems,” 1961.
- [63] P. G. Harper, “Single band motion of conduction electrons in a uniform magnetic field,” *Proceedings of the Physical Society. Section A*, vol. 68, p. 874, oct 1955.
- [64] K. Schulten and R. G. Gordon, “Exact recursive evaluation of 3j- and 6j-coefficients for quantum-mechanical coupling of angular momenta,” *Journal of Mathematical Physics*, vol. 16, pp. 1961–1970, 10 1975.
- [65] V. N. Sazonov, “Quasiclassical theory of the excitation of a quantum nonlinear oscillator,” *Theoretical and Mathematical Physics*, vol. 35, no. 3, pp. 514–520, 1978.
- [66] P. A. Braun, “Wkb method for three-term recursion relations and quasienergies of an anharmonic oscillator,” *Theoretical and Mathematical Physics*, vol. 37, no. 3, pp. 1070–1081, 1978.
- [67] P. A. Braun, “Quasienergies of an anharmonic oscillator in parametric resonance,” *Theoretical and Mathematical Physics*, vol. 41, no. 3, pp. 1060–1066, 1979.
- [68] S. Y. Chen, D. Vorobev, and G. M. Tarnopolsky *In preparation*.
- [69] H. Neuberger, “Semiclassical calculation of the energy dispersion relation in the valence band of the quantum pendulum,” *Phys. Rev. D*, vol. 17, pp. 498–506, Jan 1978.
- [70] G. V. Dunne and M. Unsal, “WKB and Resurgence in the Mathieu Equation,” 3 2016.
- [71] D. Vu and S. Das Sarma, “Moiré versus mott: Incommensuration and interaction in one-dimensional bichromatic lattices,” *Phys. Rev. Lett.*, vol. 126, p. 036803, Jan 2021.